

Impact jetting by a solid sphere

By S. T. THORODDSEN¹, T. G. ETOH²,
K. TAKEHARA² AND Y. TAKANO²

¹Mechanical Engineering, National University of Singapore, 9 Engineering Drive 1, Singapore 117576

²Civil and Environmental Engineering, Kinki University, Higashi-Osaka 577-8502, Japan

(Received 29 August 2003 and in revised form 1 November 2003)

We use a novel ultra-high-speed video camera to study the initial stage of the impact of a solid sphere onto a liquid surface, finding a high-speed horizontal jet which emerges immediately following the initial contact. For $Re > 2 \times 10^4$ the jet emerges when the horizontal contact between the sphere and the liquid is only 12% of its diameter. For the largest Reynolds numbers this jet can travel at more than 30 times the impact velocity of the sphere. This jetting occurs sooner and at much higher normalized velocities than has been observed previously. The breakup of the jet into a spray of droplets sometimes occurs through formation of pockets in the liquid sheet. Early in the impact, the energy transferred to the jet and the subsequent spray sheet is estimated to be much larger than the energy associated with the added mass inside the liquid pool. The jetting will therefore greatly increase the initial impact force on the sphere.

1. Introduction

The impact of a solid onto a liquid surface can generate high pressure and a big splash, as anyone who jumps into a swimming pool can attest to. This canonical problem is of interest in a number of areas, from water entry of missiles and the skipping of speed-boats to hydrodynamic loading on ship bows in heavy seas. The initial impact force is of interest as it can damage the solid. Experiments presented herein are conducted on the idealized water-entry problem of a solid sphere hitting a liquid surface.

The earliest systematic studies of this phenomenon were the photographs taken by Worthington at the start of the last century (Worthington 1908). His remarkable photographs revealed many of the basic phenomena of splashing. Quantitative experimental work has mainly focused on measuring the overall forces on the impacting solid and the cavity formation after it has entered far into the liquid surface, e.g. Watanabe (1934), Abelson (1970), May (1951) and May & Woodhull (1948, 1950). Experiments on the water entry of ogave bodies at various angles have been carried out by Lee & Low (1990). Moghisi & Squire (1981) measured the initial impact force directly, using a piezo-electric transducer mounted on a supported hemisphere. Their work covered a wide range of Reynolds numbers, while focusing on Re below 10^4 . This is significantly lower than the highest values in the present experiments.

Early theory on this problem was by Wagner (1932), who introduced a complex transformation now called the Wagner function, which identifies the unknown location of the free surface, as described by Dobrovolskaya (1969). His work was motivated

by the impact loading during landing and gliding of sea-planes. His theory assumes potential flow and small deformation of the free surface. This theory can therefore, in the most optimistic scenario, only be valid during the initial contact. Despite this very simplified theoretical approach the solution of the problem is difficult, principally due to the presence of the free surface, which makes the boundary conditions and flow domain part of the solution, not the problem statement. Even the most advanced mathematical attacks (Scolan & Korobkin 2001) ignore the spray jet, not allowing the free surface to become vertical. Most of the non-classified work on this problem was performed in the former Soviet Union, as reviewed by Korobkin & Pukhnachov (1988). Wedge-entry problems have been of special theoretical interest due to their geometric similarity, e.g. Hughes (1972) and references therein.

The reader should keep in mind that all the jetting phenomena discussed herein occur within 1 ms from the first contact and most within the first 100 μs . They are therefore entirely invisible to the unaided human eye, which only has a temporal resolution of the order of $1/60 \text{ s} \approx 15 \text{ ms}$, a fact exploited by television technology.

2. Experimental setup

2.1. Ultra-high-speed video camera

The key to obtaining the present measurements is the novel ultra-high-speed video camera developed by Etoh *et al.* (2002, 2003). This camera can capture at frame rates up to 1 million f.p.s. To achieve this very fast frame rate the camera uses simultaneously parallel read-out of all pixels, along with In-Situ Image Storage (ISIS) next to every pixel on the CCD chip. The prototype can acquire 103 consecutive frames. Each frame has 260×312 pixel elements irrespective of the frame rate used. The resulting image quality is far superior to the very popular C-MOS cameras developed earlier by Etoh (1992), where the number of pixels was reduced to 64×64 at the highest frame rate of 40500 f.p.s. Furthermore, the new camera does not suffer the time-shifting within frames which degrades the accuracy of the C-MOS images. The new camera records frames continually into the ISIS memory, which clears through a drain, until a trigger signal stops the imaging. This signal can be timed at any of the 103 images, even allowing observations of events which occur before the trigger signal. This flexibility is essential to deal with the temporal jitter, associated with the mechanical components of the trigger. To highlight the required accuracy of the triggering mechanism, at the highest frame rate the sphere, travelling at 9.43 m s^{-1} , will only traverse 0.96 mm during the 103 frames. The triggering consists of a laser-beam/photo-diode setup. The sphere blocks the laser beam during its fall, thus starting the camera time-delay circuit.

2.2. Experimental conditions

The experiments were conducted in the Hydraulics Laboratory at Kinki University, in a large unheated room. The room air temperature varied with the seasons between 8°C and 31°C . This variation had to be taken into account when evaluating the viscosity of the water/glycerin solutions, using curve-fits to tabulated data.

Steel spheres of three different diameters were used, with $D = 12.7, 25.4$ and 50.8 mm . Their material density was $\rho_s = 7.65 \text{ g cm}^{-3}$. The impact velocity was simply varied by changing the release height of the spheres. Release heights were in most cases around the values of 2.5 or 4.5 m, varying around those two values depending on the liquid containers used. In combination with using water or water/glycerin solutions, the

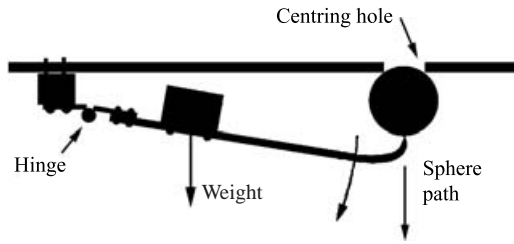


FIGURE 1. Sketch of the sphere release mechanism.

range of impact Reynolds numbers ($Re = UD/\nu$) was from 5×10^2 to 6×10^5 . Here U is the sphere impact velocity, D is its diameter and ν the kinematic viscosity of the liquid. As pointed out by Moghisi & Squire (1981) a more relevant Reynolds number should be based on the diameter of the contact, as the liquid has no knowledge of the part of the sphere which is still above water. However, as the diameter of the contact changes in time, we have here used the above definition of the Reynolds number as an overall parameter. Furthermore, as we only use spheres in the present experiments, the radius of curvature $D/2$ determines uniquely the theoretical increase in the added mass during the impact.

In all the experiments the Weber number ($We = \rho DU^2/\sigma$) was very large, greater than 10^4 . Here ρ is the liquid density and σ is the surface tension. Some reference experiments were conducted using ethyl alcohol to reduce the surface tension. The resulting Weber numbers are as high as 1.0×10^5 . Despite these extremely large Weber numbers, the effects of surface tension cannot be ignored, as the ejected liquid sheets are so thin that surface tension plays a crucial role in their breakup.

2.3. The sphere release mechanism

To observe the initial impact, it is essential to have repeatable impact conditions. This is especially true while using the fastest frame rates and largest lens magnifications. This was accomplished by constructing a special release mechanism, shown in figure 1. The horizontal position of the sphere was fixed by pressing it against a hole in a metallic plate. This plate was clamped to a structural I-beam in the ceiling of the building. Original attempts at releasing the sphere by hand, using the nail of one finger, would often impart a very slight sideways motion to the sphere, thereby changing the impact location by a few millimetres. We therefore designed a new release mechanism consisting of a hinged aluminium beam, bent at one end, where it was formed into a sharp tip. A heavy mass was placed on the beam close to the hinge. This guaranteed that the downward motion of the tip did not interfere with the free-fall of the sphere. Even though the beam was now released by hand, its trajectory was very repeatable and without generating random sideways motions of the sphere. The average horizontal deviation of the sphere from the mean impact location was 0.48 mm after falling from a release height of 4.58 m. This deviation was similar for all three sphere sizes used. Furthermore, this mechanism did not impart any rotation to the sphere. This was confirmed by observing some anomalous cases, where the sphere was not cleaned properly and small dust particles were visible adhering to its surface. The rotation rate could thus be measured from the video frames. No rotation was observed. The pixel accuracy of this measurement corresponded to the rotational surface velocity being less than 0.6% of the downward velocity of the sphere.

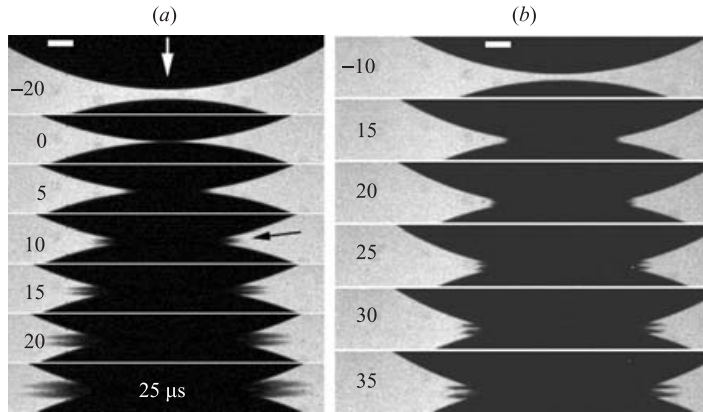


FIGURE 2. Impact jetting for 25.4 mm diameter steel sphere impacting at $U = 9.43 \text{ m s}^{-1}$, onto (a) water ($Re = 3.04 \times 10^5$) and (b) liquid of higher viscosity, 75% glycerin/water mixture at 31°C ($Re = 9.25 \times 10^3$). The lower sphere and jet images in each frame are due to reflections in the liquid surface. The scale bars are 1 mm long and the numbers indicate μs from first contact.

3. Experimental results

3.1. Initial jet speeds

The video images reveal that high-speed horizontal jetting occurs very soon after first contact. Using frame rates between 100 kHz and 1 MHz, we are able to get an accurate estimate of the emergence and initial speed of this jet. Figure 2 shows sequences of frames from typical video clips used for this purpose. In figure 2(a) the jet emerges at about $8 \mu\text{s}$ after the initial contact. During that time the sphere has only penetrated the original liquid level by $75 \mu\text{m}$.

The initial jetting speed depends primarily on the impact Reynolds number. Figure 3 shows the velocity ratio $U_{\text{jet}}/U_{\text{sphere}}$ vs. Re . The measured values of this ratio exceed 30, at the highest Re . This is about twice as large as any previous measurements, as is discussed below. It appears that Reynolds number independence has not been achieved even at these very large Re , as the normalized jetting speed has not reached a plateau.

Some additional experiments were performed using alcohol. The observed jets show similar velocities, confirming that surface tension does not play a major role in determining the initial velocity of the jet.

3.2. The emergence of the jet

Figure 4 shows the size of the horizontal contact when the jet first emerges. The jet emerges earlier as the Reynolds number increases and seems to reach an asymptote for the ratio of the horizontal contact diameter and the sphere diameter of $D_c/D \simeq 0.12 \pm 0.02$, for $Re \simeq 2 \times 10^4$. This jet therefore emerges earlier for an impacting sphere than an impacting drop, where $D_c/D = 0.21$, see Thoroddsen (2002) and Weiss & Yarin (1999).

3.3. Breakup of the jet

For the largest Re the jets are very thin and emerge horizontally very close to the free surface (figure 2a). The ‘fuzzy’ appearance in the last frames of this figure suggest it has already broken into fine spray, whereas the more viscous jet in figure 2(b) remains

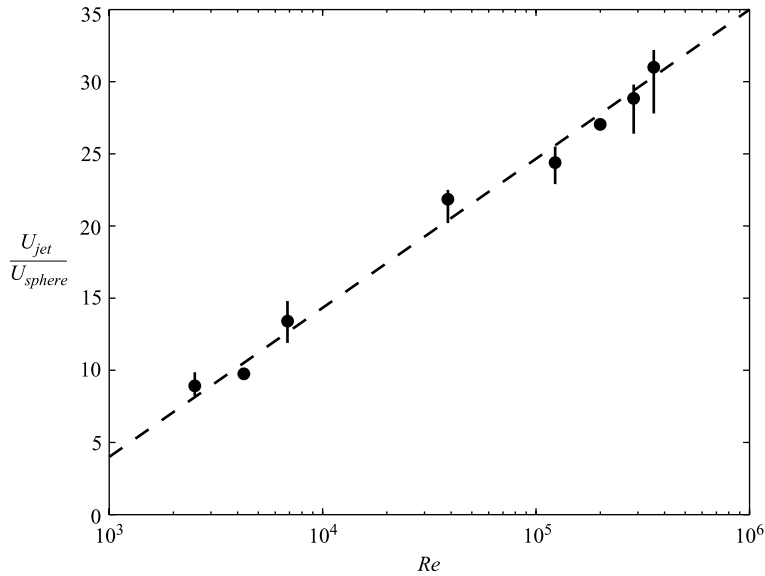


FIGURE 3. Initial jetting velocity normalized by sphere impact velocity, vs. impact Reynolds number. Data are included for steel spheres of diameters 2.54 and 5.08 cm, released from either around 2.5 or 4.5 m. The error bars show the observed range over the handful of realizations performed for each condition.

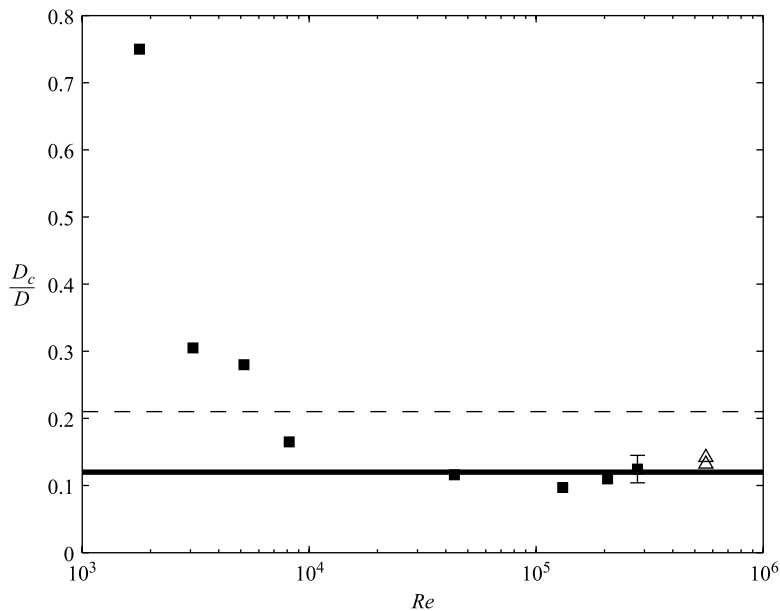


FIGURE 4. Origin of the jet for different Reynolds numbers. The figure shows the horizontal extent of the contact between the sphere and the liquid where D_c is the contact diameter and D the sphere diameter, when the jet emerges. The solid squares are for a sphere diameter $D = 25.4$ mm and the triangles for $D = 50.8$ mm. The broken line is the asymptote $D_c/D = 0.21$, which is observed for ejecta sheets under an impacting liquid drop by Thoroddsen (2002) and Weiss & Yarin (1999). The thick line is a fit to the data with $D_c/D = 0.12$.

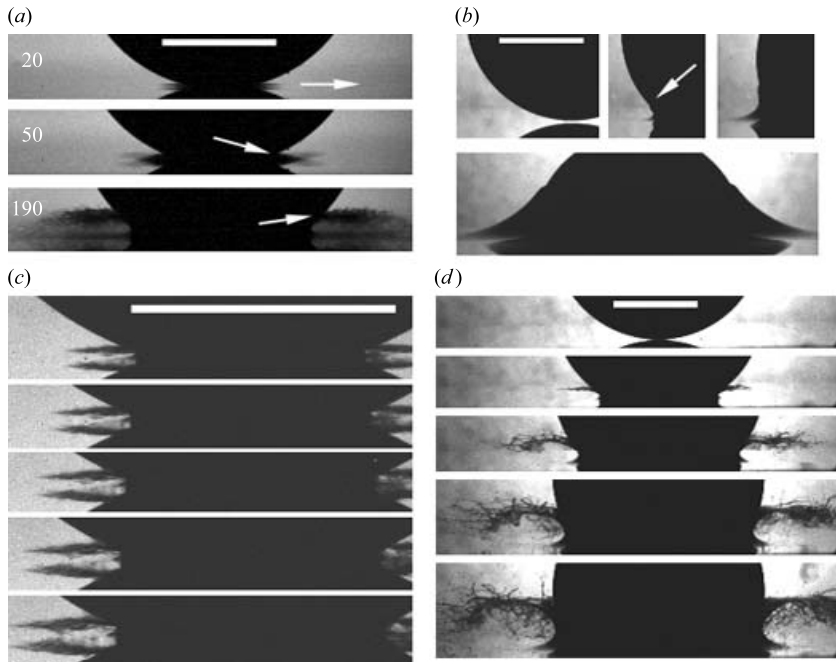


FIGURE 5. Shapes and evolution of the jets. (a) Spray jet for $Re = 1.8 \times 10^5$. (b) Lower $Re = 1.8 \times 10^3$ (90% glycerin, $D = 25.4$ mm, $U = 9.43$ m s $^{-1}$), where the jet stays attached to the sphere, arrow points to its tip. The frames correspond to -20 , 240 , 580 and 1360 μ s from first contact. (c) Intermediate $Re = 9.2 \times 10^3$. The time interval between frames is 5 μ s. (d) Irregular breakup of the jet into spray, $Re = 3078$. The frames are spaced by 150 μ s. The scale bars are 10 mm long.

intact. Figure 5(a) shows the early evolution of this fine spray. The video reveals that the originally horizontal spray is subsequently directed slightly downwards from the sphere surface towards the pool liquid, before reversing and heading upwards, as the spray root has travelled further up the sphere surface.

For the lowest Reynolds numbers the jet travels along the sphere surface without separation, as shown in figure 5(b). For intermediate viscosities the jet separates from the sphere forming an irregular surface as shown in figure 5(c,d). This shape may be produced by an irregular contact line on the surface of the sphere, where the sheet emerges. The irregular location of the contact line is for example clearly visible in US Navy photographs, reproduced by Batchelor (1967, plate 18). In figure 5(d) the breakup of the jet into fine droplets takes place by repeated formation of hollow pockets in the sheet, as it travels against the air pressure. Figure 6 shows the formation and breakup of such a pocket of diameter about 0.8 mm. This breakup of the sheet tends to leave extended tendrils, as shown in the last panel of figure 6.

4. Discussion and conclusions

4.1. Jetting velocities

The highest jetting velocities observed herein are approximately 300 m s $^{-1}$, giving normalized values U_{jet}/U_{sphere} much larger than have been observed in any previous experiments, even for higher Mach number impacts. The ingenious gel experiments of Field, Lesser & Dear (1985) at impact Mach numbers of 0.1 show jetting at

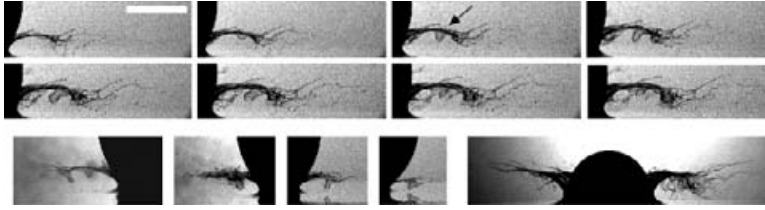


FIGURE 6. Breakup of the liquid jet by formation of a finger-like hollow pocket, marked by the arrow, $Re = 2700$, $We = 4.2 \times 10^4$ (75% glycerin solution at 10°C). The time interval between frames in the top row is $50\ \mu\text{s}$ and the second row $20\ \mu\text{s}$, showing the breakup by a hole forming at the bottom of the finger. The scale bar is 5 mm. The bottom row shows other examples of such pockets and the resulting outwards shooting of tendrils. The sphere in the last panel has $D = 25.4\ \text{mm}$.

a maximum of 17 times the impact velocity. Similar experiments of Dear & Field (1988) show a ratio of 12. The theory of Lesser (1981) predicts that the jetting depends strongly on the angle of the solid with the liquid and is in good agreement with the gel experiments. The very high impact velocities used in those experiments ($U = 150\ \text{m s}^{-1}$) make imaging particularly difficult, which may lead to some underestimation of the earliest jetting speeds. However, this jetting is clearly affected by the liquid compressibility and its nature appears much different from ours (see figures 4 and 9 in Field *et al.* 1985). This jetting appears as spray generated by ‘spallation’ of the drop liquid and the emerging droplets bounce between the solid and liquid surfaces. The viscoelastic properties of the gel may also play a role.

Recently discovered ejecta sheets (Thoroddsen 2002), arising when a drop impacts onto a liquid layer, emerge from the pool liquid at slightly more than 10 times U , with drops emerging at as much as 13 times U for $Re = 2.9 \times 10^4$. This is significantly lower than observed herein for the solid sphere.

Despite the high jet velocities observed herein, they are still well below the sound speed in water and compressibility effects are therefore negligible, as discussed in Lesser & Field (1983). The supersonic duration of the impact can be estimated by the speed of the outwards motion of the contact line between the sphere and the liquid surface. Using the simple geometry of the intersection point between a flat plane and a circle, we obtain the outwards motion and velocity of the contact point:

$$x_c(t) = \sqrt{Ut(2R - Ut)} \quad \Rightarrow \quad V_c(t) = \frac{dx_c}{dt} = \frac{UR - U^2t}{\sqrt{Ut(2R - Ut)}}.$$

For the earliest times, where t is very small, $V_c \approx \sqrt{UR/2t}$. The speed of the outwards motion of the contact line, for this simplified geometry, is therefore infinite at $t = 0$. However, for the largest sphere used here ($D = 50.8\ \text{mm}$), V_c has reduced to the speed of sound in water ($c \sim 1500\ \text{m/s}$) after $0.05\ \mu\text{s}$. We can therefore conclude that the emergence of the jet, at $t \approx 10\ \mu\text{s}$ is purely an incompressible phenomenon. This is further supported by the fact that for the more viscous liquids, the jet persists, but emerges even later, at $19\ \mu\text{s}$ in figure 2(b). In other words, we cannot use the water-hammer pressure $\sim \rho Uc$ (Cook 1928) to explain the high speed of the jet.

The observed high-speed jetting is therefore more likely to be rooted in an incompressible mechanism akin to the inviscid potential theory initiated by Wagner (1932). He looked at the self-similar impact of a two-dimensional wedge onto a liquid layer, predicting infinite velocities rising up a wide-angle wedge in a ‘spray tip’. Much theoretical effort has been devoted to eliminating this singularity, see the discussion

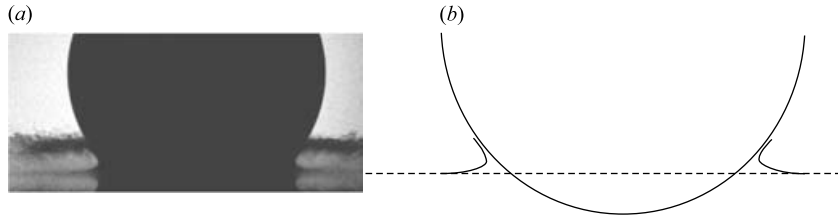


FIGURE 7. Surface shape and spray jet for water. The sphere penetration depth is $B/R = 0.22$. (a) Video frame taken $300 \mu\text{s}$ after first contact, for $D = 25.4 \text{ mm}$ and $U = 9.43 \text{ m s}^{-1}$, $Re = 1.8 \times 10^5$. (b) Surface shape and sphere penetration digitized from the video image in (a) at a magnified scale.

in Hughes (1972). The no-slip condition at the sphere surface and the formation of a boundary layer makes such details irrelevant to the present study. However, by approximating our sphere by a large-angle cone, this theory clearly suggests the possibility of high-speed jetting without recourse to any compressibility effects.

4.2. The force of impact

The force of impact on the sphere arises primarily through the transfer of kinetic energy to the liquid. Figure 7 shows a typical spray jet for a high- Re impact. The fraction of energy carried away from the impact by this spray is determined by its velocity and the mass of liquid contained in it. Once the spray root rises up the side of the sphere, we can observe the shape of the free surface. Figure 7(b) shows its trace, with the outline of the sphere. This allows us to estimate what fraction of the displaced liquid goes into the swell and, by subtraction, how much liquid ends up in the spray. In this particular image about $58 \pm 15\%$ of the displaced liquid has ended up in the spray jet, with the uncertainty arising mainly from determining the water level away from the sphere. The bulk volume of the spray-disk is approximately 4 times the volume displaced by the sphere, thus giving the volume fraction of the droplets in the spray as 15%.

The added mass of the pool liquid, as the sphere penetrates the free surface, can be modelled using the potential flow around a lens, as done by Shiffman & Spencer (1947). This added mass is determined by the ratio of the penetration depth B and radius of the disk of horizontal contact R_c . For small ratios $b = B/R_c$ the added mass resembles that of a flat disk, $2/\pi$ (Lamb 1932, p. 129), whereas for $b = 1$, the added mass takes the value for a sphere, 0.5.

The contact radius in figure 7 is $R_c/R = 0.63$ and penetration $B = 0.22 R$. From Shiffman & Spencer (1947) (their figure 9) the added mass coefficient for a lens with $b = 0.35$ becomes

$$M = 0.68 \rho \pi R_c^3 = 0.51 \rho \frac{4}{3} \pi R_c^3.$$

Here we need to halve these values, as we ignore the mass of the air and the swell. The volume of the sphere of radius R_c is here 7.3 times larger than the displaced volume, giving the ratio of spray mass to added mass of $0.58 / (7.3 \times 0.5 \times 0.51) = 0.312$.

We can now compare the kinetic energy in the liquid pool to the kinetic energy carried by the spray jet. The average speed of the spray in figure 7 is estimated from the video as 5.3 times the sphere velocity. This gives the ratio of the two kinetic energies as

$$\frac{T_{\text{spray}}}{T_{\text{pool}}} = \frac{M_{\text{spray}}}{M_{\text{pool}}} \left(\frac{v_{\text{spray}}}{v_{\text{sphere}}} \right)^2 = 8.8.$$

This suggests that about 90% of the kinetic energy transferred from the sphere to the liquid appears in the spray jet. This implies that the drag calculated using the potential flow past a lens could underestimate the initial drag by an order of magnitude. Note that our estimate ignores the kinetic energy of the liquid contained in the swell. Scolan & Korobkin (2001) anticipate possible errors due to ignoring the spray jet in their theoretical treatment of the slamming problem, but not as large as these results might indicate.

During the earliest stages, when the largest jet velocities are observed, the jet velocity is as much as 30 times larger than the sphere velocity. Assuming the same liquid fractions as above, this would channel over 99% of the energy into the spray jet.

The experiments of Moghisi & Squire (1981) focused mostly on the lower range of Re studied herein, finding drag coefficients in good agreement with the potential theory of Shiffman & Spencer (1947). However, from the rough estimates above, it becomes clear that the initial impact force and flow field during water entry problems, at high Reynolds numbers cannot be accurately studied by ignoring the spray jet in the analysis. Direct measurements of the earliest impact force at high Re should clarify this issue and pinpoint the significance of these jets.

In conclusion, we have used a novel ultra-high-speed video camera to study the initial stage of the impact of a solid sphere onto a liquid surface. We find that, for high Reynolds number impacts, fluid jetting occurs much earlier and at much higher speeds than previously thought. We have also discovered a new breakup mechanism for the ejected liquid sheets, through the formation of finger-like pockets. We propose that this early jetting will significantly affect the initial force of impact on the sphere, which questions the accuracy of theoretical models, which invariably ignore this jetting.

S. T. T. was supported by a JSPS fellowship during his first visit to Kinki University.

REFERENCES

- ABELSON, H. I. 1970 Pressure measurements in the water-entry cavity. *J. Fluid Mech.* **44**, 129–144.
- BATCHELOR, G. K. 1967 *An Introduction to Fluid Dynamics*. Cambridge University Press.
- COOK, S. S. 1928 Erosion by water-hammer. *Proc. R. Soc. Lond. A* **119**, 481–488.
- DEAR, J. P. & FIELD, J. E. 1988 High-speed photography of surface geometry effects in liquid/solid impacts. *J. Appl. Phys.* **63**, 1015–1021.
- DOBROVOLSKAYA, Z. N. 1969 On some problems of similarity flow of fluid with a free surface. *J. Fluid Mech.* **36**, 805–829.
- ETOH, T. G. 1992 High speed camera of 4500 pps. *J. Inst. Television Engrs, Japan* **45**, 534–545 (in Japanese).
- ETOH, T. G., POGGEMANN, D., KREIDER, G. *et al.* 2003 An image sensor which captures 100 consecutive frames at 1000000 frames/s. *IEEE Trans. Electron Devices* **50**, No. 1, 144–151.
- ETOH, T. G., POGGEMANN, D., RUCKELSHAUSEN, A. *et al.* 2002 A CCD image sensor of 1 M frames/s for continuous image capturing of 103 frames. *2002 IEEE Intl Solid-State Circuits Conf. Digest of Technical Papers*, vol. 45, pp. 46–47.
- FIELD, J. E., LESSER, M. B. & DEAR, J. P. 1985 Studies of two-dimensional liquid-wedge impact and their relevance to liquid-drop impact problems. *Proc. R. Soc. Lond. A* **401**, 225–249.
- HUGHES, O. F. 1972 Solution of the wedge entry problem by numerical conformal mapping. *J. Fluid Mech.* **56**, 173–192.
- KOROBKIN, I. I. & PUKHNACHOV, V. V. 1988 Initial stage of water impact. *Annu. Rev. Fluid Mech.* **20**, 159–185.
- LAMB, H. 1932 *Hydrodynamics*. Cambridge University Press.

- LEE, T. S. & LOW, H. T. 1990 Water entrance characteristics of a 60° truncated ogive nose projectile. *J. Inst. Engrs, Singapore (IES)* **30**, 49–55.
- LESSER, M. B. 1981 Analytical solutions of liquid-drop impact problems. *Proc. R. Soc. Lond. A* **377**, 289–308.
- LESSER, M. B. & FIELD, J. E. 1983 The impact of compressible liquids. *Annu. Rev. Fluid Mech.* **15**, 97–122.
- MAY, A. 1951 The effect of surface conditions of a sphere on its water-entry cavity. *J. Appl. Phys.* **22**, 1219–1222.
- MAY, A. & WOODHULL, J. C. 1948 Drag coefficients of steel spheres entering water vertically. *J. Appl. Phys.* **19**, 1109–1121.
- MAY, A. & WOODHULL, J. C. 1950 The virtual mass of a steel spheres entering water vertically. *J. Appl. Phys.* **21**, 1285–1289.
- MOGHISI, M. & SQUIRE, P. T. 1981 An experimental investigation of the initial force of impact on a sphere striking a liquid surface. *J. Fluid Mech.* **108**, 133–146.
- SCOLAN, Y.-M. & KOROBKIN, A. A. 2001 Three-dimensional theory of water impact. Part 1. Inverse Wagner problem. *J. Fluid Mech.* **440**, 293–326.
- SHIFFMAN, M. & SPENCER, D. C. 1947 The flow of an ideal incompressible fluid about a lens. *Q. Appl. Maths* **5**, 270–288.
- THORODDSEN, S. T. 2002 The ejecta sheet generated by the impact of a drop. *J. Fluid Mech.* **451**, 373–381.
- TRILLING, L. 1950 The impact of a body on a water surface at an arbitrary angle. *J. Appl. Phys.* **21**, 161–170.
- WAGNER, H. 1932 Uber Stoss-und Gleitvorgange an der Oberfluche von Flussigkeiten. *Z. Angew. Math. Mech.* **12**, 193–215.
- WATANABE, S. 1934 Resistance of impact on water surface. Part V - sphere. *Inst. Phys. Chem. Res. Sci. Papers* **484**, 202–208.
- WEISS, D. A. & YARIN, A. L. 1999 Single drop impact onto liquid films: neck distortion, jetting, tiny bubble entrainment, and crown formation. *J. Fluid Mech.* **385**, 229–254.
- WORTHINGTON, A. M. 1908 *A Study of Splashes*. Longmans (Reprinted 1963, Macmillan).